Applied Catalysis B: Environmental 193 (2016) 9–15

Contents lists available at ScienceDirect

Applied Catalysis B: Environmental

journal homepage: www.elsevier.com/locate/apcatb

Iron incorporation on graphene nanoflakes for the synthesis of a non-noble metal fuel cell catalyst

Pierre-Alexandre Pascone*, Jasmin de Campos, Jean-Luc Meunier, Dimitrios Berk

Plasma Processing Laboratory (PPL), McGill University, Chemical Engineering, 3610 University Street, Montreal, Québec H3A 0C5, Canada

ARTICLE INFO

Article history:
Received 23 October 2015
Received in revised form 30 March 2016
Accepted 1 April 2016
Available online 2 April 2016

Keywords:
Graphene
Nanomaterial
Catalyst
Oxygen reduction reaction
Nitrogen functionalization

ABSTRACT

In the present work, graphene nanoflakes (GNFs) were grown at both low and high levels of nitrogen functionalization and subsequently put through a wet-chemical method to add iron functionalities to the surface and create active catalyst centers. No mechanical treatments are used in order to minimize the formation of defects on the GNFs and evaluate if iron-nitrogen-GNF edges or surface sites can generate catalytic activity rather than the macropore structures holding these functionalities on porous carbon black. The catalysts produced under various synthesis routes were characterized and screened for their performance as an oxygen reduction reaction (ORR) catalyst. Characterization included an electrochemical study, an examination of the carbon and nitrogen content and bonding structure, in addition to Raman analysis and the calculation of the BET surface areas. It was found that samples that were both treated with iron acetate and put through pyrolysis produced the most active samples. These samples were composed of graphitic carbon and contained a large amount of pyridinic nitrogen. Additionally, when working with GNFs generated with high levels of nitrogen, no extra nitrogen source was needed during the iron incorporation step. This study further develops the GNF-based catalyst already seen to be a suitable ORR catalyst for the polymer electrolyte membrane fuel cell.

1. Introduction

Graphene, an atomic layer of carbon atoms in a two-dimensional aromatic ring matrix, has attracted much attention as a material due to its large surface area and high electrical conductivity [1]. This material has potential applications in varying fields, such as nanofluids [2], supercapacitors [3], and fuel cells [4]. Producing high quality and purity graphene was shown to be possible by Prisitavita et al. by the thermal decomposition of a carbon feedstock in a thermal plasma [5]. The produced graphene, called graphene nanoflakes (GNFs) powder, has a structure that is characterized by a stacking of roughly 5–15 graphene planes of typical planar dimensions of 100 by 100 nm. The GNFs are considered graphene rather than graphite because the properties of single-layer graphene, such as the length scale of the stacked crystalline planes, persist within this material [6]. The resulting powder is extremely pure and contains little to no amorphous carbon, in addition to having a very high degree of crystallinity and being chemically resistant to acidic and basic environments.

Depending on the plasma conditions during GNF growth, nitrogen can be attached at various levels reaching up to above 30 atomic percent on the surface with a fraction of around 25% of this nitrogen being in pyridinic sites of the graphene structure [7]. By introducing iron into the nitrogen functionalized GNFs through a wet-chemical method outside the plasma reactor, a catalyst for the oxygen reduction reaction (ORR) can be crafted. For the catalyst to be effective, the iron should be bound to nitrogen atoms which are part of the graphitic structure. The key to obtaining a high catalytic activity for ORR is in the nature of the iron-nitrogen-carbon bond, and whether there is pyridinic or pyrrolic nitrogen. The evaluation of the iron active site is still under investigation in the research community with pyrrolic nitrogen being associated with higher activity, but pyridinic nitrogen being associated with decreased peroxide formation and increased energy efficiency [8].

For the specific applications of alkaline fuel cells (AFCs) and polymer electrolyte membrane fuel cells (PEMFCs), platinum, an expensive precious metal, is typically used as a catalyst for the ORR. Non-noble metals, particularly cobalt and iron, atomically dispersed on carbon nanomaterials show promise as platinum cathode catalyst replacements for both PEMFCs [9–24] and AFCs [25–33].

* Corresponding author.
E-mail addresses: pierrealexandre.pascone@mail.mcgill.ca (P.-A. Pascone), jasmin.decampos@mail.mcgill.ca (J. de Campos), jean.luc.meunier@mcgill.ca (J.-L. Meunier), dimitrios.berk@mcgill.ca (D. Berk).

http://dx.doi.org/10.1016/j.apcatb.2016.04.002
0926-3373/

In this work, GNFs were produced with varying amounts of nitrogen functionalization and used as the carbon base onto which iron could be atomically dispersed. The synthesis parameters were varied and the resulting catalysts were fully characterized by their elemental composition, crystallinity, in addition to being tested for their ability to reduce oxygen in neutral media.

The iron-incorporation method used in this work has been adapted for the GNFs from an existing process developed by Dodelet et al. Their work used carbon black particles as the carbon precursor, and iron acetate and phenanthroline were then added as their iron and nitrogen sources respectively [34–40]. They then tuned the porosity of carbon black particles and filled the pores using a ball milling step and a two-stage pyrolysis. The catalytic activities of these structures were very close to matching those of platinum while the amount of defects and specific porosity of the carbon black particles seem to play a major role in attaining the high level of catalytic activity. A microscale porosity was induced on the carbon black structures used by Lefèvre et al. for creating the porphyrin-like catalytic sites through mechanical/thermal treatments [36–39]. The catalytic stability of these structures over time, however, remains problematic, and the increased crystallinity of the carbon structures was observed to correlate with stability improvement of the catalyst [40]. The requirement of defects and porous sites on the carbon black support proved to be necessary for the formation the iron-nitrogen-carbon catalytic sites, while such defects are not involved at the same level on the highly crystalline graphene structures for the generation of such sites.

We may thus hypothesize that further increasing the crystallinity level through the use of graphene-based materials hosting the iron-nitrogen-carbon catalytic sites would present a promising avenue for providing both activity and stability. The ball milling treatment and pyrolysis procedure presented by Jaouen et al. [34] was first used unchanged on our GNFs in a preliminary study [41]. Although the low iron content yielded the expected relatively low activity levels, the catalyst produced did show catalytic stability during a 100-h PEMFC test [41]. Optimization of iron incorporation levels onto our GNFs is now required to enhance their catalytic performance while maintaining the integrity of the graphene structure.

In using the mechanical/thermal treatments of Lefèvre et al. on the GNFs for the synthesis of the catalyst, we noted from Raman spectroscopy that the graphene structures showed a significant reduction of the crystallinity parameters [41]. Instead of forming the macropore structures holding the functionalities on porous carbon black, one objective here is to prevent the formation of defects on the pure GNFs and form the catalytic sites on the GNF edges; thus the ball milling step that follows the addition of iron acetate and phenanthroline has been omitted in the new set of experiments presented here. Additionally, since the GNFs already contain nitrogen, the ammonia pyrolysis stage is removed, and the temperature of the argon pyrolysis is lowered to minimize damage to the GNFs. The main objective of this work is to investigate the role of iron acetate, phenanthroline, and pyrolysis as synthesis steps and determine their effect on the catalyst structure and activity towards reducing oxygen.

2. Experimental

2.1. Graphene nanoflakes growth

The GNF powders are produced by the plasma decomposition of methane and their surface is functionalized with nitrogen [5,7]. The plasma parameters used to grow the different GNFs are shown in Table 1. In this work, two distinct levels of nitrogen functionalization are used: low (0.5 to 3 atomic percent of nitrogen on the surface) and high (15 to 25 atomic percent of nitrogen on the surface).

Table 1
GNF growing parameters.

Stage	Low Nitrogen (LN-GNFs)		High Nitrogen (HN-GNFs)	
Preparation	Power	20 kW	Power	20 kW
	Pressure	13.79 kPa	Pressure	13.79 kPa
	Argon	64.5 slpm	Argon	64.5 slpm
	Time	5 min	Time	5 min
Growth	Power	20 kW	Power	20 kW
	Pressure	55.16 kPa	Pressure	55.16 kPa
	Argon	64.5 slpm	Argon	64.5 slpm
	Methane	1 slpm	Methane	1 slpm
	Nitrogen	0.1 slpm	Nitrogen	0.1 slpm
	Time	20 min	Time	10 min
Functionalization			Power	25 kW
			Pressure	13.79 kPa
			Argon	15 slpm
			Nitrogen	50 slpm
			Time	30 min

Table 2
Conditions for samples produced.

Sample Name	Nitrogen Amount	Iron Acetate	Phenanthroline	Pyrolysis
HN-0	High			
HN-1	High	√		
HN-2	High	√		√
HN-3	High		√	
HN-4	High		√	√
HN-5	High	√	√	
HN-6	High	√	√	√
LN-0	Low			
LN-1	Low	√		
LN-2	Low	√		√
LN-3	Low		√	
LN-4	Low		√	√
LN-5	Low	√	√	
LN-6	Low	√	√	√

2.2. Catalyst synthesis

The low nitrogen (LN) and high nitrogen (HN) GNFs are further treated outside the plasma reactor to form the catalyst by adding iron using iron acetate and/or nitrogen using phenanthroline. The GNFs are mixed in a 1 to 1 volume ratio of ethanol and water in an ultrasonic cleaner for 1 h. In cases where phenanthroline is added, a 1 to 1 mass ratio is used with GNFs. Iron acetate is added to the solution to obtain 1% mass of iron within the solid mixture. After mixing, the solution is transferred to an oven and heated to 105 °C until all the liquid evaporates and the dried sample is then collected. At this stage, the sample is pyrolyzed to promote the incorporation of atomically dispersed iron. Pyrolysis is carried out using argon gas at a flow rate of 600 sccm and a temperature of 700 °C for 1 h. Following pyrolysis, no further treatments are performed. A series of 14 samples were prepared under various precursor and process combinations in order to evaluate the possible effects of the synthesis procedure. Table 2 illustrates the different conditions used to produce the samples in this work. The sample numbers presented in this table will be used for identification purposes.

2.3. Characterization techniques

An electrochemical study using a rotating disk electrode (RDE) was conducted as a screening technique to determine which samples stood out as suitable catalyst candidates for reducing oxygen.

For these tests we have chosen a neutral solution to follow the work done by Amirfakhri et al. on the catalytic ORR [42]. If the synthesized catalysts are to be used in PEMFCs and AFCs, experiments in acidic and alkaline solutions will have to be performed to assess their activities and stabilities under those conditions. However, it is already known from previous work that the GNF-based catalysts are suitable for the acidic environments of PEMFCs [41].

The GNF samples are dispersed in an ink made up of Nafion™, water, and ethanol. To prepare the ink, the GNFs are mixed in a 4 to 1 volume ratio of water and ethanol at a concentration of 1 mg per mL, and a 5 wt percent Nafion™ solution is added at 4 μL per mg of GNF. The ink is sonicated in an ice bath for 1 h, deposited on a glassy carbon RDE tip to obtain a concentration of 0.1 mg of GNFs per cm^2 of electrode, and dried in a humid environment at 65 °C until the liquid evaporates. After drying, the tips are examined under a microscope to confirm uniform coverage. The tip is used as the working electrode in a 0.1 M sodium sulfate neutral solution, with an oxygen and argon gas mixture being bubbled into solution in order to obtain a concentration near 32 mg of oxygen per litre. A rotation rate of 2500 rpm and a scan rate of 10 mV/s were used in the RDE experiments.

All the GNF samples are characterized using X-ray photoelectron spectroscopy (XPS) to determine the elemental composition on their surface. XPS is performed on a Scientific K-Alpha XPS system from Thermo Scientific with an aluminium x-ray source, 300 μm spot size, and Avantage 5.932 software. Additionally, Raman spectroscopy is performed to study the graphitic content of the samples. The Raman instrument used in the present project is an inVia Reflex confocal micro-Raman (Renishaw) with a laser emitting at a wavelength of 514.5 nm. All peak intensities and areas are measured using the Wire 2.0 software. Finally, the Brunauer-Emmett-Teller (BET) area is calculated by an Autosorb iQ Gas Sorption machine from Quantachrome Instruments. Nitrogen is used as the analysis gas with a bath temperature of 77.35 K. The BET area of each sample is calculated by generating a multi-point BET plot and focusing on the relative pressures in the range of 0.05–0.3.

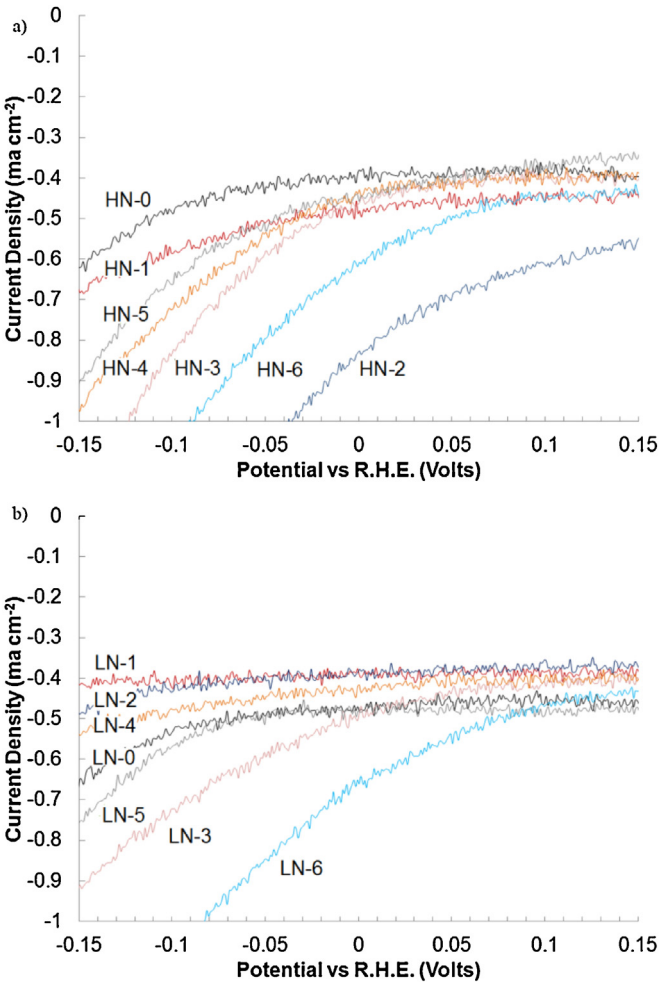

Fig. 1. Current density vs R.H.E. for (a) low nitrogen samples and (b) high nitrogen samples.

3. Results and discussion

3.1. Catalytic activity

The best method to determine the performance of a catalyst for fuel cell applications is through tests in a real fuel cell environment; however, these tests are costly, time consuming, and require a great use of resources. Instead of testing all the samples produced in this study in a fuel cell, an electrochemical study with RDE is performed as a screening technique to determine which candidates merit a more vigorous investigation. The RDE study may also provide information on the reaction mechanism and kinetics. The ORR occurring at the cathode of the cell is the slowest and limiting reaction and requires the highest load of catalyst; attention is thus given primarily to this ORR reaction. The GNF samples were studied here using RDE focussing on the range from 0.15 V to −0.15 V vs RHE, which corresponds to the region right before the 2-electron electrochemical reduction of oxygen with the superoxide anion as the intermediate, and the current density was measured with respect to the applied voltage (Fig. 1) [22].

The electrocatalytic activity is equivalent to the rate of reduction of oxygen in this case which is proportional to the current. The cathodic nature of the reaction shows here the currents as negative values. Therefore the lowest curves in Fig. 1(a and b) represent the samples with the strongest catalytic performance. To better illustrate the performance of the samples, the values at 0 V for each sample were gathered over many runs (Fig. 2).

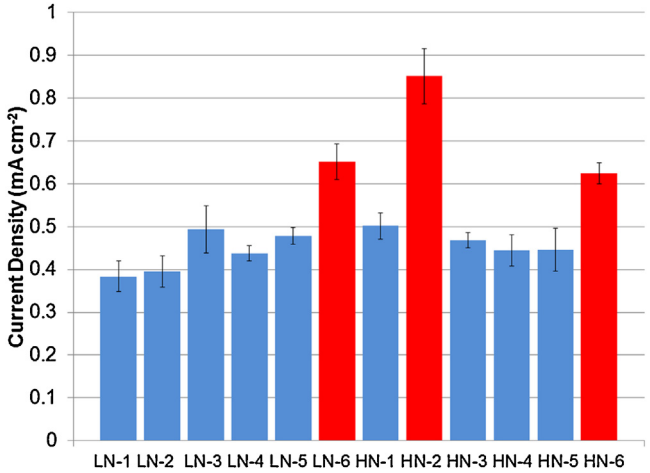

Fig. 2. Absolute value of current density at 0 V vs R.H.E.

All samples demonstrate some level of activity, including the untreated samples (LN-0 and HN-0), with the activity of the LN-0 sample towards the reduction of hydrogen peroxide already having been demonstrated in previous work [42]. The GNFs have a catalytic effect on the reduction reaction, but the aim is to improve the activity of the untreated samples by incorporating iron, phenanthroline, and performing pyrolysis. In Fig. 2, most of the samples were at

the level between 0.4 and 0.5 mA cm^{-2}, making them statistically similar to one another and not significantly greater than untreated GNFs. Three samples stood out with higher activities, namely sample numbers HN-2, HN-6, and LN-6. The best performance was that of the HN-2 at a value of 0.851 mA cm^{-2}. The activity value of HN-2 compares favorably with other non-platinum catalysts, such as carbon supported manganese oxide nanoparticles [16] and beanpod-shaped Fe-C-N composites [23], which fall in the range of 0.2–2.8 mA cm^{-2}; however, these studies do not clearly report the amount of catalyst material used during experiments, making a normalized comparison on the basis of mass hard to do. The HN-2 catalyst was able to achieve a high activity in a neutral solution with a relatively small loading. In a study by Wu et al. that investigated the electrochemical reduction of oxygen catalyzed by reduced graphene sheets in neutral media, they report a value of around 0.75 mA cm^{-2}, but their experiments used double the catalyst loading than in our experiments [22]. The fact that HN-2's performance already surpasses other non-platinum catalysts in the literature is a good sign for its future as an ORR catalyst.

Fig. 2 also provides information on the effect of using iron acetate, phenanthroline, and the use of a pyrolysis step. As expected none of the four iron-free samples (LN-3, LN-4, HN-3, HN-4) stand out in terms of activity, because iron is the active component of this catalyst. These results further exemplify the importance of iron acetate to the catalyst synthesis procedure. When comparing all the iron-containing samples, the pyrolyzed samples (LN-2, LN-6, HN-2, HN-6) produced a higher current density than their respective un-pyrolyzed counterparts (LN-1, LN-5, HN-1, HN-5). In fact, the iron-containing samples that have not experienced pyrolysis are statistically equivalent to the iron-free samples and the untreated GNFs. The three most active samples in this study (red columns in Fig. 2: LN-6, HN-2, HN-6) went through a pyrolysis process. This result shows the importance of the pyrolysis step for proper iron incorporation. The chemical composition and physical phase of the GNFs can be irreversibly changed to incorporate the atomically dispersed iron on the surface of the graphene sheets.

Focusing on the iron-containing samples and comparing the phenanthroline-free samples (LN-1, LN-2, HN-1, HN-2) to the phenanthroline-containing samples (LN-5, LN-6, HN-5, HN-6), one sees the presence of phenanthroline increases the current density of the LN-GNF samples whereas it is decreasing it for HN-GNFs. It appears that the LN-GNFs do not have enough nitrogen present initially, phenanthroline acting as an extra nitrogen source for them. However, for HN-GNFs, the nitrogen is already at a very high loading on the GNF surface following the plasma process; the addition of phenanthroline is not seen to improve the catalyst activity. Contrary to the carbon black material and catalyst preparation technique used by the team of Dodelet et al., phenanthroline can be omitted from the iron incorporation step altogether because the carbon nanomaterial precursor already has the proper nitrogen content to form an active catalyst.

The surface area of the untreated GNFs and the three most active samples were measured by the BET method to further validate the RDE results. The results presented in Figs. 1 and 2 are normalized with respect to the area of the RDE disc, but since each sample is prepared at the same concentration and the same volume is deposited, it is equivalent to normalization with respect to mass. By determining the surface area, this mass can be converted into a 'GNF surface area' and the results can be re-evaluated to determine if they still are statistically different from the control case of untreated GNFs. The area calculation will vary depending on whether the sample is in powder form or dispersed in an ink, but it is assumed that the differences between the samples are relatively similar for either condition. In the present work, the area was measured in powder form for comparison reasons. All the samples produced a fairly similar BET surface area, which is shown in Table 3. These results were then used to re-normalize the RDE values, also presented in Table 3. When these new values are considered, the active samples still stand out among the rest, further confirming the RDE results.

Table 3
Current density normalized with 'GNF surface area'.

Sample Name	Current Density w/'geometric area' [mA cm^{-2}]	BET Surface Area [m^2 g^{-1}]	Current Density w/'GNF surface area' [mA m^{-2}]
HN-0	0.454	211	21.51
HN-2	0.851	209	40.62
HN-6	0.625	174	35.97
LN-0	0.448	182	24.62
LN-6	0.651	178	36.56

Table 4
Elemental atomic percent from surface analysis.

Sample Name	Carbon[atomic percent]	Nitrogen[atomic percent]
HN-0	74.16	20.60
HN-1	78.62	17.41
HN-2	**93.03**	**4.28**
HN-3	76.27	19.90
HN-4	89.83	8.54
HN-5	80.04	14.24
HN-6	**90.23**	**6.02**
LN-0	97.92	0.74
LN-1	95.88	1.15
LN-2	98.81	0.38
LN-3	97.59	1.26
LN-4	95.60	2.96
LN-5	92.85	3.95
LN-6	**94.13**	**3.84**

Knowing the BET surface area is also useful for comparing this material to similar materials being used by other research groups where values can range from 400 to 1800 m^2 per g [43–46]. The results obtained in this study may seem to be low especially when compared to the 'perfect case' of graphene. By assuming a unit cell of one benzene ring with a bond length of 0.142 nm, one-sixth of a carbon atom at each vertex (or one atom per ring), and a mass of 2×10^{-23} g per atom, one obtains a surface area of 2619 m^2 per g, which matches the literature quite well [47]. The GNFs produced in this work had a surface area less than one-tenth of the calculated value, but the GNFs contain nitrogen, iron, oxygen, and may not be perfect aromatic rings; each of these defects adds mass to the structure and decreases the surface area value. Defects are sought in our catalyst structure as we want iron-nitrogen-GNF edges to be potential active sites. A relatively low BET surface area is a good sign for our catalyst.

3.2. Elemental composition

All produced samples were characterized by XPS to evaluate the overall content of nitrogen; in addition, a deconvolution of the peaks was performed to attribute the elemental signals to bond types. The results of the two primary peaks, carbon and nitrogen, are shown in Table 4 with the three most active samples from the RDE study (HN-2, HN-6, and LN-6) shown in bold. The other elemental signals in the samples were iron, when applicable, in small amounts (less than 0.5 atomic percent) and oxygen (1.5 to 5 atomic percent).

The HN-GNFs produced in this work had a nitrogen content of about 20 atomic percent on the surface before being treated. There is a noticeable difference between the pyrolyzed (HN-2, HN-4, and HN-6) and non-pyrolyzed samples (HN-1, HN-3, and HN-5). Pyrolysis always resulted in at least a 58 percent decrease

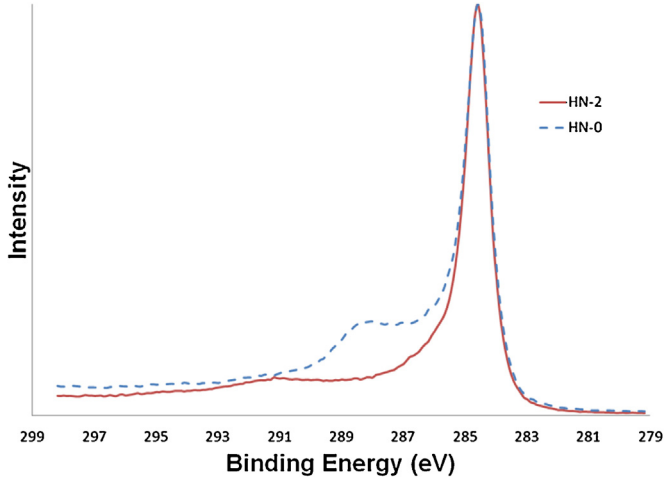

Fig. 3. XPS of carbon peak for HN-0 and HN-2.

of the nitrogen content; for the case in which only iron acetate was added (HN-1 and HN-2), a 75 percent decrease was observed. This result indicates that, with the untreated HN-GNFs, a large amount of nitrogen might be attached to amorphous carbon and the pyrolysis procedure breaks these bonds, leading to the sharp decrease in nitrogen content. For the LN-GNFs, the original nitrogen content was very low (less than 1 atomic percent), but in all the cases where phenanthroline was added (LN-3, LN-4, LN-5, and LN-6), the nitrogen content increased significantly, even by more than 400 percent for the lone active low nitrogen sample (LN-6 compared to LN-0).

When examining the carbon and nitrogen signals of all the samples, the three most active samples from the RDE study (HN-2, HN-6, LN-6) produced similar signals to one another, exhibiting the same overall shape and relative bond types, although with differing amounts of total nitrogen and carbon for both the low and high nitrogen cases. All other samples produced the same XPS spectra for carbon and nitrogen as untreated GNFs (HN-0 and LN-0). Fig. 3 shows the carbon signal of the most active sample (HN-2) compared to the untreated HN-GNFs (HN-0). The main carbon peak is at a binding energy of 284.6 eV and the peak of HN-2 is slightly less broad than that of HN-0, best illustrated in the binding energy of 285–287 eV, indicating slightly less amorphous carbon [48]. At the binding energies of 287–291 eV are the signals for functional group attachments. HN-2 and HN-0 both give a signal in this range, but that of HN-2′s is at a lower intensity, symbolizing that the functional groups are attaching to graphitic carbon and not amorphous carbon. This decrease in amorphous carbon content for the three most active samples means that they contain an overall higher graphitic content and are therefore a purer material, which increases their catalytic activity towards the ORR.

Fig. 4 shows the nitrogen signals for HN-0 and HN-2. The two cases have noticeably different shapes. HN-0 produces a symmetrical nitrogen signal, with 32 percent being attributed to the pyridinic peak (binding energy of approximately 398.7 eV), while HN-2 has a noticeable slant to a lower binding energy and 70 percent of the signal coming from the pyridinic peak. The high pyridinic content is desirable for the specific application of PEMFCs, but the lack of pyrrolic nitrogen (binding energy of approximately 400.3 eV) likely indicates a low overall activity.

3.3. Crystallinity

The Raman spectra for each of the samples in this study were obtained and analyzed. Indices for the purity, the crystallite size, and the average length of graphene planes provide a better understanding of the nature of the graphitic content through examination of the three main peaks [49–52]. The calculated values for these factors for the three most active samples are presented in Table 5. It can be observed again here that sample HN-2 stands out. The addition of iron acetate to the HN-GNFs still maintains a high purity factor, with an average length of graphene plane that almost doubles the two other samples. In comparison, when the unmodified incorporation method of Jaouen et al. is used on GNFs, the average length of the graphene planes is around 10 nm by the end of the second pyrolysis step [41]. By using HN-GNFs and eliminating phenanthroline, ball milling, and one pyrolysis stage from the iron incorporation method, the damaging of the graphene sheets is minimized.

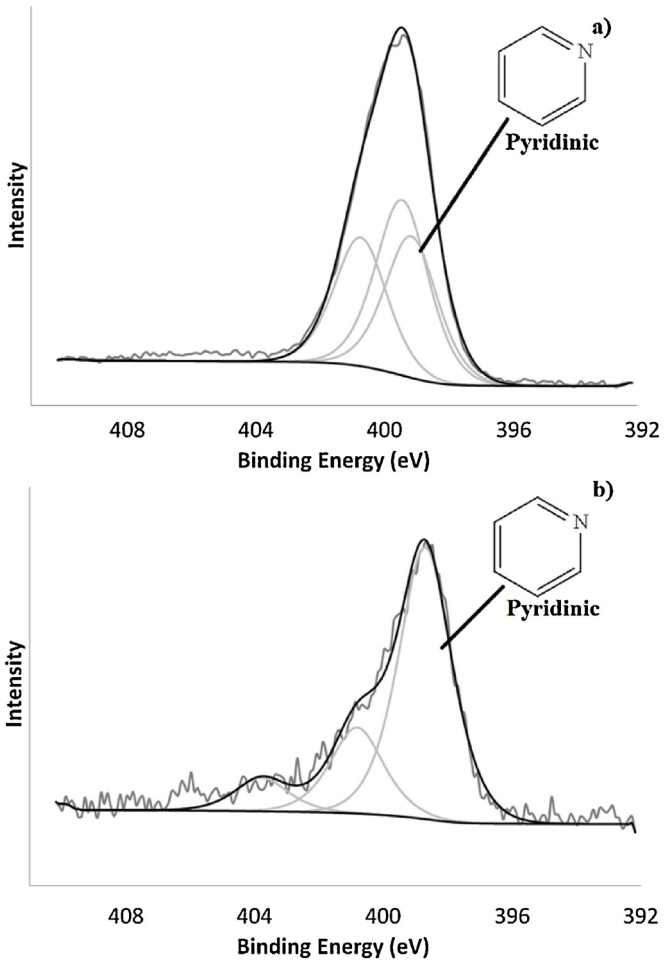

Fig. 4. XPS of nitrogen peak for a) HN-0 and b) HN-2.

Table 5
Crystallinity parameters.

Sample Name	Purity	Crystallite Size [nm]	Average Length of Graphene Plane [nm]
HN-2	2.37 ± 0.06	6.86 ± 0.15	18.51 ± 0.92
HN-6	1.82 ± 0.10	5.76 ± 0.54	8.87 ± 0.21
LN-6	2.11 ± 0.07	7.37 ± 0.48	9.72 ± 1.43

Raman performed on the samples demonstrated an interesting property that further helps reinforce the importance of pyrolysis for the iron incorporation step. When the HN-GNF samples are treated with iron, phenanthroline, or both, they all give off a fluorescent signal in their Raman spectra. However, the fluorescence is eliminated by performing pyrolysis. Fig. 5 shows this result for the HN-GNF

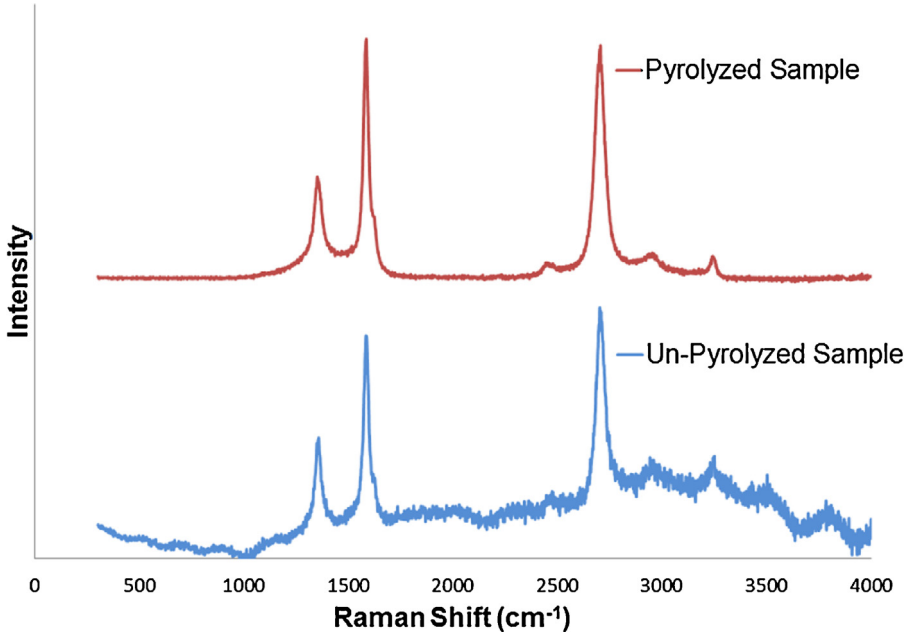

Fig. 5. Raman spectra of HN-GNFs with iron before (HN-1) and after (HN-2) pyrolysis.

with iron. This seems to show that poly-aromatic hydrocarbons are formed by the iron incorporation steps and then removed by pyrolysis, yielding a cleaner material.

4. Conclusions

GNFs grown in a thermal plasma reactor at two nitrogen levels were treated with iron acetate, phenanthroline, and a pyrolysis step in order to optimize their catalytic activity. It was found through RDE, XPS, Raman, and BET analysis that iron acetate and pyrolysis were essential components for the incorporation of iron onto the GNFs. Additionally, pyrolysis is required as a final step for iron incorporation as it improves the activity while removing the fluorescence of the samples. By altering the nitrogen levels of the nanomaterial, it was found that phenanthroline was not needed for GNF samples containing a high level of nitrogen by plasma functionalization, but helped the GNF samples generated with a low level of nitrogen to obtain a higher activity. The carbon and nitrogen signals also showed that the catalyst having the highest activity also have the highest level of graphitization and the majority of their nitrogen in pyridinic states. This study provides results towards optimizing the iron incorporation process for GNFs and eventually developing a suitable non-noble metal ORR catalyst. With the untreated GNFs already providing some activity for ORR, a relatively small amount of atomically dispersed iron added onto the GNFs is shown here to double this initial activity level. Studies on the active site and the position of the atomically dispersed iron within the catalysts are currently underway, in addition to actual fuel cell testing.

Acknowledgments

The authors would like to acknowledge the funding contributions of the *Fonds de Recherche Nature et Technologie du Québec* (FRNTQ) and the *Natural Science and Engineering Research Council* (NSERC) of Canada. Additionally, Pierre-Alexandre Pascone would like to thank David Morris for his help with the BET machine and Ulrich Legrand for useful discussions.

References

[1] A.K. Geim, A.H. MacDonald, Graphene: exploring carbon flatland, Phys. Today 60 (2007) 35–41.
[2] U. Legrand, N.-Y. Mendoza Gonzalez, P. Pascone, J.-L. Meunier, D. Berk, Synthesis and in-situ oxygen functionalization of deposited graphene nanoflakes for nanofluid generation, Carbon 102 (2016) 216–223.
[3] A. Yoo, J.J. Balakrishnan, K. Huang, J. Meunier, V. Sumpter, B.G. Strivastava, Ultrathin planar graphene supercapacitors, Nano Lett. 11 (2011) 1423–1427.
[4] L. Qu, Y. Liu, J.B. Baek, L. Dai, Nitrogen-doped graphene as efficient metal-free electrocatalyst for oxygen reduction in fuel cells, ACS Nano 4 (2010) 1321–1326.
[5] R. Pristavita, J.L. Meunier, D. Berk, Carbon nano-flakes produced by an inductively coupled thermal plasma system for catalyst applications, Plasma Chem. Plasma Process. 31 (2011) 393–403.
[6] N. Larouche, B.L. Stansfield, Classifying nanostructured carbons using graphitic indices derived from Raman spectra, Carbon 48 (2010) 620–629.
[7] D.M. Binny, J.L. Meunier, D. Berk, Nitrogen doping of graphene nanoflakes by thermal plasma as catalyst for oxygen reduction in Proton Exchange Membrane fuel cells, Proc. IEEE Conf. Nanotechnol. (2012) 8–13.
[8] Y. Shao, J. Sui, G. Yin, Y. Gao, Nitrogen-doped carbon nanostructures and their composites as catalytic materials for proton exchange membrane fuel cell, Appl. Catal. B Environ. 79 (2008) 89–99.
[9] G. Faubert, R. Côté, D. Guay, J.P. Dodelet, G. Dénès, P. Bertrandc, Iron catalysts prepared by high-temperature pyrolysis of tetraphenylporphyrins adsorbed on carbon black for oxygen reduction in polymer electrolyte fuel cells, Electrochim. Acta 43 (1998) 341–353.
[10] C. Han, X. Bo, Y. Zhang, M. Li, A. Wang, L. Guo, Dicobalt phosphide nanoparticles encased in boron and nitrogen co-doped graphitic layers as novel non-precious metal oxygen reduction electrocatalysts in alkaline media, Chem. Commun. 51 (2015) 15015–15018.
[11] F. Jaouen, J. Herranz, M. Lefèvre, J.-P. Dodelet, U.I. Kramm, I. Herrmann, et al., Cross-laboratory experimental study of non-noble-metal electrocatalysts for the oxygen reduction reaction, ACS Appl. Mater. Interfaces 1 (2009) 1623–1639.
[12] R. Jasinski, A new fuel cell cathode catalyst, Nature 201 (1964) 1212–1213.
[13] M. Manzoli, F. Boccuzzi, Characterisation of Co-based electrocatalytic materials for O_2 reduction in fuel cells, J. Power Sources 145 (2005) 161–168.
[14] C. Médard, M. Lefèvre, J.P. Dodelet, F. Jaouen, G. Lindbergh, Oxygen reduction by Fe-based catalysts in PEM fuel cell conditions: activity and selectivity of the catalysts obtained with two Fe precursors and various carbon supports, Electrochim. Acta 51 (2006) 3202–3213.
[15] T.S. Olson, S. Pylypenko, J.E. Fulghum, P. Atanassov, Bifunctional oxygen reduction reaction mechanism on non-platinum catalysts derived from pyrolyzed porphyrins, J. Electrochem. Soc. 157 (2010) B54–B63.
[16] I. Roche, K. Scott, Carbon-supported manganese oxide nanoparticles as electrocatalysts for oxygen reduction reaction (orr) in neutral solution, J. Appl. Electrochem. 39 (2009) 197–204.
[17] Y. Si, Z. Xiong, X. Liu, M. Li, A highly active nitrogen-containing non-precious metal catalyst CoHMTA/C for oxygen reduction reaction, Int. J. Electrochem. Sci. 10 (2015) 5212–5221.

[18] R. Sirirak, T. Sarakonsri, M. Medhesuwakul, Non-platinum nanocatalyst on porous nitrogen-doped carbon fabricated by cathodic vacuum arc plasma technique, Appl. Surf. Sci. 356 (2015) 512–520.
[19] S. Tang, H. Huangfu, Z. Dai, L. Sui, Z. Zhu, Preparation of Fe-N-Carbon nanocoils as catalyst for oxygen reduction reaction, Int. J. Electrochem. Sci. 10 (2015) 7180–7191.
[20] G. Wang, W. Wang, L.-K. Wang, W.-T. Yao, P.-F. Yao, W.-K. Zhu, et al., A N-, Fe- and Co-tridoped carbon nanotube/nanoporous carbon nanocomposite with synergistically enhanced activity for oxygen reduction in acidic media, J. Mater. Chem. A 3 (2015) 17866–17873.
[21] G. Wu, K.L. More, C.M. Johnston, P. Zelenay, High-performance electrocatalysts, Science 332 (2011) 443–448.
[22] J. Wu, Y. Wang, D. Zhang, B. Hou, Studies on the electrochemical reduction of oxygen catalyzed by reduced graphene sheets in neutral media, J. Power Sources 196 (2011) 1141–1144.
[23] Z.-Y. Yang, Y.-X. Zhang, L. Jing, Y.-F. Zhao, Y.-M. Yan, K.-N. Sun, Beanpod-shaped Fe–C–N composite as promising ORR catalyst for fuel cells operated in neutral media, J. Mater. Chem. A 2 (2014) 2623–2627.
[24] X. Zhang, W. Ouyang, D. Zeng, Y. Zhan, F. Xie, W. Zhang, et al., Nitrogen doped sublimed carbon as non-noble metal catalyst for oxygen reduction reaction, Catal. Today (2015).
[25] F. Bidault, D.J.L. Brett, P.H. Middleton, N.P. Brandon, Review of gas diffusion cathodes for alkaline fuel cells, J. Power Sources 187 (2009) 39–48.
[26] Q. He, Q. Li, S. Khene, X. Ren, F.E. Lopez-Suarez, D. Lozano-Castello, et al., High-loading cobalt oxide coupled with nitrogen-doped graphene for oxygen reduction in anion-exchange-membrane alkaline fuel cells, J. Phys. Chem. C 117 (2013) 8697–8707.
[27] I. Kruusenberg, L. Matisen, Q. Shah, A.M. Kannan, K. Tammeveski, Non-platinum cathode catalysts for alkaline membrane fuel cells, Int. J. Hydrogen Energy 37 (2012) 4406–4412.
[28] M. Liu, R. Zhang, W. Chen, Graphene-supported nanoelectrocatalysts for fuel cells: synthesis, properties, and applications, Chem. Rev. 114 (2014) 5117–5160.
[29] R. Liu, D. Wu, X. Feng, K. Müllen, Nitrogen-doped ordered mesoporous graphitic arrays with high electrocatalytic activity for oxygen reduction, Angew. Chem. Int. Ed. 49 (2010) 2565–2569.
[30] Z. Mo, S. Liao, Y. Zheng, Z. Fu, Preparation of nitrogen-doped carbon nanotube arrays and their catalysis towards cathodic oxygen reduction in acidic and alkaline media, Carbon 50 (2012) 2620–2627.
[31] K. Niu, B. Yang, J. Cui, J. Jin, X. Fu, Q. Zhao, et al., Graphene-based non-noble-metal Co/N/C catalyst for oxygen reduction reaction in alkaline solution, J. Power Sources 243 (2013) 65–71.
[32] E.H. Yu, X. Wang, U. Krewer, L. Li, K. Scott, Direct oxidation alkaline fuel cells: from materials to systems, Energy Environ. Sci. 5 (2012) 5668.
[33] E.H. Yu, U. Krewer, K. Scott, Principles and materials aspects of direct alkaline alcohol fuel cells, Energies 3 (2010) 1499–1528.
[34] F. Jaouen, M. Lefèvre, J.-P. Dodelet, M. Cai, Heat-treated Fe/N/C catalysts for O_2 electroreduction: are active sites hosted in micropores? J. Phys. Chem. B 110 (2006) 5553–5558.
[35] F. Jaouen, S. Marcotte, J.P. Dodelet, G. Lindbergh, Oxygen reduction catalysts for polymer electrolyte fuel cells from the pyrolysis of iron acetate adsorbed on various carbon supports, J. Phys. Chem. B 107 (2003) 1376–1386.
[36] M. Lefèvre, J.P. Dodelet, P. Bertrand, O_2 Reduction in PEM fuel cells: activity and active site structural information for catalysts obtained by the pyrolysis at high temperature of Fe precursors, J. Phys. Chem. B 104 (2000) 11238–11247.
[37] M. Lefèvre, J.P. Dodelet, Fe-based electrocatalysts made with microporous pristine carbon black supports for the reduction of oxygen in PEM fuel cells, Electrochim. Acta 53 (2008) 8269–8276.
[38] M. Lefèvre, J.-P. Dodelet, P. Bertrand, Molecular oxygen reduction in PEM fuel cells: evidence for the simultaneous presence of two active sites in Fe-based catalysts, J. Phys. Chem. B 106 (2002) 8705–8713.
[39] M. Lefèvre, E. Proietti, F. Jaouen, J.-P. Dodelet, Iron-based catalysts with improved oxygen reduction activity in polymer electrolyte fuel cells, Science 324 (2009) 71–74.
[40] E. Proietti, F. Jaouen, M. Lefèvre, N. Larouche, J. Tian, J. Herranz, et al., Iron-based cathode catalyst with enhanced power density in polymer electrolyte membrane fuel cells, Nat. Commun. 2 (2011) 416–424.
[41] P.-A. Pascone, D. Berk, J.-L. Meunier, A stable and active iron catalyst supported on graphene nano-flakes for the oxygen reduction reaction in polymer electrolyte membrane fuel cells, Catal. Today 211 (2013) 162–167.
[42] S.J. Amirfakhri, P.-A. Pascone, J.-L. Meunier, D. Berk, Fe–N-doped graphene as a superior catalyst for H_2O_2 reduction reaction in neutral solution, J. Catal. 323 (2015) 55–64.
[43] N. Larouche, R. Chenitz, M. Lefèvre, E. Proietti, J.P. Dodelet, Activity and stability in proton exchange membrane fuel cells of iron-based cathode catalysts synthesized with addition of carbon fibers, Electrochim. Acta 115 (2014) 170–182.
[44] V.H. Luan, H.N. Tien, L.T. Hoa, N.T.M. Hien, E. Oh, J.S. Chung, et al., Synthesis of a highly conductive and large surface area graphene oxide hydrogel and its use in a supercapacitor, J. Mater. Chem. A 1 (2013) 208–211.
[45] M.A. Worsley, S.O. Kucheyev, H.E. Mason, M.D. Merrill, B.P. Mayer, J. Lewicki, et al., Mechanically robust 3D graphene macroassembly with high surface area, Chem. Commun. 48 (2012) 8428–8430.
[46] S. Yang, L. Zhi, K. Tang, X. Feng, J. Maier, K. Müllen, Efficient synthesis of heteroatom (N or S)-doped graphene based on ultrathin graphene oxide-porous silica sheets for oxygen reduction reactions, Adv. Funct. Mater. 22 (2012) 3634–3640.
[47] M.D. Stoller, S. Park, Y. Zhu, J. An, R.S. Ruoff, Graphene-based ultracapacitors, Nano Lett. 8 (2008) 3498–3502.
[48] NIST X-ray Photoelectron Spectroscopy Database, Version 4.1 (National Institute of Standards and Technology, Gaithersburg, 2012), (n.d.). http://srdata.nist.gov/xps/.
[49] C. Castiglioni, C. Mapelli, F. Negri, G. Zerbi, Origin of the D line in the Raman spectrum of graphite: a study based on Raman frequencies and intensities of polycyclic aromatic hydrocarbon molecules, J. Chem. Phys. 114 (2001) 963–974.
[50] A. Cuesta, P. Dhamelincourt, J. Laureyns, A. Martinez-Alonso, J.M.D. Tascon, Comparative performance of X-ray diffraction and Raman microprobe techniques for the study of carbon materials, J. Mater. Chem. 8 (1998) 2875–2879.
[51] T. Jawhari, A. Roid, J. Casado, Raman spectroscopic characterization of some commercially available carbon black materials, Carbon 33 (1995) 1561–1565.
[52] Y. Wang, D.C. Alsmeyer, R.L. Mccreery, Raman spectroscopy of carbon materials: structural basis of observed spectra, Chem. Mater. 2 (1990) 557–563.